graphic analysis, where hypothesized globally synchronous sea level cycles form the basis of the popular paradigm of sequence stratigraphy.

REFERENCES AND NOTES

1. As opposed to the specific layered-silicate mineral glauconite, the term "glaucony" is used as a facies term for the family of marine Fe-rich minerals ranging in composition from glauconitic smectite to glauconitic mica.
2. G. J. Wasserburg, R. J. Hayden, J. Jensen, *Geochim. Cosmochim. Acta* **10**, 153 (1956).
3. See, for example, J. D. Obradovitch, *Paleoceanography* **3**, 757 (1988).
4. G. S. Odin, Ed., *Green Marine Clays* (Elsevier, Amsterdam, 1988).
5. _____, Ed., *Numerical Dating in Stratigraphy* (Wiley-Interscience, New York, 1982), part 1, pp. 151–454.
6. _____, *ibid*., pp. 387–403.
7. _____, *C. R. Acad. Sci. Paris* **318**, 59 (1994).
8. W. A. Berggren, D. V. Kent, J. J. Flynn, J. A. Van Couvering, *Geol. Soc. Am. Bull.* **96**, 1407 (1985).
9. Recoil loss of ^{39}Ar previously prohibited the application of ^{40}Ar-^{39}Ar ages to clay minerals. The problem was overcome by use of a grain encapsulation technique [P. E. Smith, N. M. Evensen, D. York, *Geology* **21**, 41 (1993)].
10. Samples: 385a (K-Ar age = 20.5 ± 0.5 Ma); 132a (K-Ar age = 40.8 ± 1.3 Ma); and GL-O (K-Ar age = 95.0 ± 0.6 Ma, 1σ). Mineralogy and stratigraphy are as described in (*5*).
11. Standard and sample grains were placed in pure quartz tubing (diameter, 1 mm) and attached to a quartz manifold evacuated to a pressure of $\sim 10^{-8}$ torr. Each sample tube was hand-held while heating the top to detach the ampoule from the manifold, ensuring minimal sample heating. Ampoules were loaded together with flux monitors of Hb-3gr hornblende (assumed age, 1071 Ma) in capsules and irradiated for 24 hours (48 MWh) in position 5C of the McMaster Nuclear Reactor, Hamilton, Ontario. Recoiled Ar gas associated with each sample was measured after breaking the ampoule under high vacuum using a custom-designed crushing apparatus and admitting the released gas into a high-sensitivity mass spectrometer. The grain was then fused using a 20-W continuous Ar-ion laser to measure Ar remaining in the sample. Our experiments have not detected any radiogenic ^{40}Ar leakage from the grain to the ampoule before or during irradiation. Therefore, all glaucony ages were calculated by integrating the recoiled ^{39}Ar in the ampoule with the data from the residual grain.
12. The uncertainty is the standard error of the mean. The age distributions represent the point-by-point sum of the probability densities of each individual age analysis. Although the curves for each age analysis have equal area, more precisely determined ages give more pronounced spikes, whereas ages with higher uncertainties appear as broader, lower-amplitude deflections. A quantitative measure of the degree to which *n* individual ages are scattered in a population, taking into account their individual experimental uncertainties, is given by $S/(n-1)$, where S is the sum of squares of the weighted deviates about the mean age. This has an expected value of 1 for a data set where no significant age variability can be detected. The value of this quantity for TCR is 0.96, indicating that we have detected no significant age variation of this standard within the limits of our experimental procedure. The weighted mean age is identical to the currently accepted age of 27.92 Ma for this standard [A. Baksi, *Eos* **73**, 328 (1992)].
13. The $S/(n-1)$ values of 6.2 for 385a, 2.8 for 132a, and 6.9 for GL-O confirm that significant age variability exists in the three populations.
14. W. B. Harland *et al*., *A Geological Time Scale 1989* (Cambridge Univ. Press, Cambridge, 1989).
15. The high-temperature minerals are derived worldwide from any level within that stage, an interval of 4 Ma or more.
16. Older ages of 25.6 ± 0.4 Ma for 385a and 99.2 ± 0.5 Ma for GL-O (Table 1) from grains having anomalously rough surface textures suggest an extraformational origin.
17. A. Cox and G. D. Dalrymple, *J. Geophys. Res.* **72**, 2603 (1967).
18. The conventional K-Ar method requires tens of milligrams of sample, comprising thousands of glaucony grains, for adequate analytical precision and to obtain representative aliquots for separate K analysis. The wide range of single-grain ages for the glaucony populations shows that such multigrain ages [including all those in the Harland *et al*. database (*14*)] must average heterogeneous grains with distinct histories and thus have limited precise significance. Furthermore, because the majority of grains in these populations are significantly younger than the depositional age of their host sediments, the averages tend to be young, which provides an explanation for the age biases in glaucony K-Ar ages used to construct the geologic time scale. (Even heterogeneous age distributions will yield reproducible K-Ar ages when thousands of grains are averaged.)
19. Because immature glauconies have thinner subgrain laminae, they would be most sensitive to Ar loss. According to a model of Ar recoil in thin parallel laminae (*9*), grains with thinner laminae also undergo greater ^{39}Ar recoil losses. Thus, if all the younger ages result from ^{40}Ar loss, they may be expected to be inversely correlated with their ^{39}Ar recoil loss. In the clay mineral illite, such a relation was attributed to low-temperature loss of both ^{39}Ar and ^{40}Ar from similar lattice sites [H. Dong, C. M. Hall, D. R. Peacor, A. N. Halliday, *Science* **267**, 355 (1995)]. In contrast, there is no simple relation between ^{39}Ar recoil and apparent age in the glaucony populations (Table 1).
20. Although this estimate is uncertain because of the difficulty in obtaining representative averages for small samples in heterogeneous populations, this method mitigates the extra uncertainties (that is, the 2% accuracy of the ^{40}Ar-^{39}Ar ages based on the age of flux monitors) involved in a comparison with the published bulk K-Ar determinations.
21. J. P. Morton and L. E. Long, *J. Sediment. Petrol.* **54**, 495 (1984).
22. B. U. Haq, J. Hardenbol, P. R. Vail, *Science* **235**, 1156 (1987). These curves were constructed according to the hypothesis that stratigraphic sequences are controlled primarily by changes in global sea level. Although this model has received much support [for instance, K. G. Miller *et al*., *ibid.* **271**,1092 (1996)], it has also encountered numerous challenges, particularly by F. M. Gradstein *et al*. [*ibid.* **241**, 599 (1988)], who pointed out that the stratigraphic uncertainties of the higher-frequency cycles (1 to 3 Ma) making up the seawater curves are currently too high to permit a test of whether they were globally synchronous.

23. We thank C. M. Hall and an anonymous reviewer for their constructive comments. Supported by an operating grant from the Natural Sciences and Engineering Research Council of Canada (D.Y.).

20 October 1997; accepted 29 January 1998

Distribution of *Thiobacillus ferrooxidans* and *Leptospirillum ferrooxidans*: Implications for Generation of Acid Mine Drainage

Matthew O. Schrenk, Katrina J. Edwards,* Robert M. Goodman, Robert J. Hamers, Jillian F. Banfield

Although *Thiobacillus ferrooxidans* and *Leptospirillum ferrooxidans* are widely considered to be the microorganisms that control the rate of generation of acid mine drainage, little is known about their natural distribution and abundance. Fluorescence in situ hybridization studies showed that at Iron Mountain, California, *T. ferrooxidans* occurs in peripheral slime-based communities (at pH over 1.3 and temperature under 30°C) but not in important subsurface acid-forming environments (pH 0.3 to 0.7, temperature 30° to 50°C). *Leptospirillum ferrooxidans* is abundant in slimes and as a planktonic organism in environments with lower pH. *Thiobacillus ferrooxidans* affects the precipitation of ferric iron solids but plays a limited role in acid generation, and neither species controls direct catalysis at low pH at this site.

A fundamental component of the sulfur geochemical cycle is the release of sulfate into solution through oxidative dissolution of sulfide minerals. Because sulfides are at least a minor component of most rocks, this process is almost ubiquitous in chemical weathering. Weathering of sulfide-rich rocks with low neutralization capacity forms sulfuric acid–rich solutions that can carry high metal loads. When ore bodies are exposed by mining, this results in an environmental condition known as acid mine drainage (AMD).

Pyrite (FeS_2) is the most abundant sulfide mineral in Earth's crust. Exposure of pyrite surfaces to oxygen and water results in the formation of sulfuric acid. Ferric iron, an abundant alternative electron acceptor in many AMD solutions, interacts effectively with surface sulfur species (*1*) and pro-

M. O Schrenk and K. J. Edwards, Department of Geology and Geophysics, University of Wisconsin–Madison, 1215 West Dayton Street, Madison, WI 53706, USA.
R. M. Goodman, Department of Plant Pathology, University of Wisconsin–Madison, 1630 Linden Drive, Madison, WI 53706, USA.
R. J. Hamers, Department of Chemistry, University of Wisconsin–Madison, 1101 University Avenue, Madison, WI 53706, USA.
J. F. Banfield, Department of Geology and Geophysics, University of Wisconsin–Madison, 1215 West Dayton Street, Madison, WI 53706, USA.

*To whom correspondence should be addressed. E-mail: katrina@geology.wisc.edu

motes pyrite dissolution by the following reaction: $FeS_2 + 14\ Fe^{3+} + 8\ H_2O \rightarrow 15\ Fe^{2+} + 2\ SO_4^{2-} + 16\ H^+$ (*2*). Microorganisms greatly accelerate the rate of oxidation of Fe^{2+} to Fe^{3+}, so that the rate of pyrite dissolution is generally controlled by microbial activity (*2–4*).

Numerous studies have measured and compared the abiotic, biotic, and Fe^{3+}-induced rates of pyrite dissolution (*2*). Almost all experimental work has used *Thiobacillus ferrooxidans*, which is generally assumed to be the most important species accelerating the dissolution of metal sulfide (*2*). *T. ferrooxidans* is considered typical of AMD systems because it can be readily cultured from these environments. The importance of the iron-oxidizing species *Leptospirillum ferrooxidans* is now also widely accepted (*5*), and this species can outcompete *T. ferrooxidans* under certain conditions (*6*, *7*). However, few studies have evaluated the potential geochemical impact of *L. ferrooxidans* in natural low-pH environments, and the distribution and abundance of these species have not been quantified.

We used molecular methods based on small-subunit ribosomal RNA (SSU rRNA) sequences (*8*) without prior cultivation (*9*) to study the role of microorganisms in an AMD environment at Iron Mountain, California, and to analyze the abundance and distribution of *T. ferrooxidans* and *L. ferrooxidans* as a function of geochemical and physical conditions. To determine the absolute contribution of these two bacterial species to the total microbial population, we evaluated the proportion of all cells in the domains Bacteria, Eukarya, and Archaea.

Iron Mountain is an in inoperative mine containing tens of kilometers of underground tunnels running through a sulfide ore body, as well as several runoff streams peripheral to the ore body. Pyrite-dominated sediments and solutions draining from the sulfide deposit were collected from the Richmond mine in January 1997. A few samples of seepage from tailings piles and storage tanks for AMD runoff from outside the mine (pH 2 to 4, temperature 10° to 25°C) were also collected and fixed for subsequent microbiological analysis (*10*).

The geochemical analyses from all sites fall into two clusters. Solutions with pH 1.5 to 2.5, temperature 17° to 30°C, and conductivity <30 mS/cm were confined to regions of the main tunnel and occasional pools. Solutions with pH 0.3 to 1.0, temperature 33° to 50°C, and conductivity >68 mS/cm were typical of most sites in contact with the ore body. Dissolved oxygen contents were higher in the higher temperature, lower pH regions, at ~1.2 mg/liter at ~20°C to ~5.2 mg/liter. This is probably due to higher mixing that occurs at spillways.

Total cell counts were determined by DNA staining with 4′, 6-diamidino-2-phenylindole (DAPI) (*7*) (Fig. 1). Cell numbers for rRNA probe–labeled samples relative to total cells were determined by dual counting of samples with differently labeled probes. Totals for the three domains should sum to the total detected with DAPI. In general, the total number of cells detected with rRNA probes was lower than that detected with DAPI, probably because some cells were dead or inactive.

The A and C drifts are two of four horizontal tunnels that diverge from the horizontal Richmond entrance tunnel about 450 m into the mine. Solutions draining from, or collecting in, the A drift had temperatures between 42° and 45°C and pH values of 0.5 to 0.7. In the C drift, the temperature was 47° to 48°C and the pH was 0.4 to 0.6. Samples from all environments were found to contain abundant microbial life. In the A and C drifts, typical direct cell counts were 2.5×10^5/ml in solutions, 1.6×10^9/ml in slime streamers, and 4.2×10^6/ml in pyrite sediment.

Cells in sediment, water, or slime that hybridized with the *T. ferrooxidans* probe were completely absent. The probe effectively hybridized with cultured *T. ferrooxidans* cells [American Type Culture Collection (ATCC) number 19859], both in solution and on pyrite surfaces. The conclusion that *T. ferrooxidans* is not important in environments typified by the A and C drifts is supported by the absence of this species in enrichment cultures that used samples from the A drift as inoculum in standard *T. ferrooxidans* media (*4*). We found that in all cases, bacteria were the predominant form of microbial life (at least 75% of cells). Eukarya were minor constituents of many assemblages but ranged up to 25% of cells in some slimes. Archaea were a minor component in solutions.

The abundance of *L. ferrooxidans* in the A and C drifts varied with microenvironment (Fig. 1). This species accounted for almost the entire bacterial component of some slimes and was present in flowing and stagnant water (Fig. 2). *Leptospirillum ferrooxidans* has been cultured as a planktonic organism from these sites (*11*). Although only a few of the bacteria in sediments are *L. ferrooxidans*, this species occurs in relatively high numbers associated with, but unattached to, the sediments (~10^5 cells/ml). Enrichment cultures also contained bacillus-shaped cells that colonized pyrite surfaces and hybridized with the bacterial probe (Fig. 3) but not with the *L. ferrooxidans* or *T. ferrooxidans* probe. We have shown that the acidophilic mesothermophilic bacteria in these cultures are chemolithotrophic, metabolize ferrous iron, and accelerate pyrite dissolution rates (~10^{-5} μmol of Fe per cell per day at

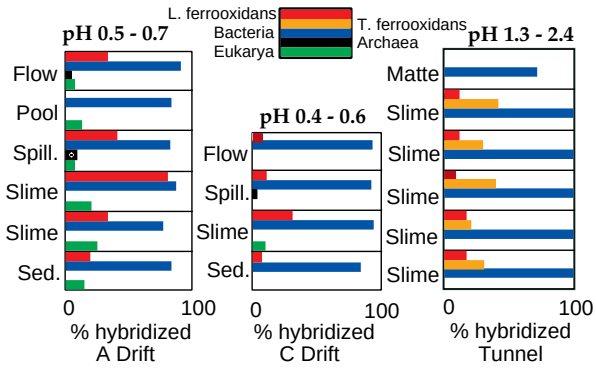

Fig. 1. Results from fluorescence in situ hybridization analysis (total cell counts determined by DNA staining with DAPI). The term "flow" refers to moving water, "pool" to standing water, "spill" to water actively flowing over a barrier in the Richmond ore body, "slime" to slime streamers on and in pools of standing water, and "sed." to sediment consisting of pyrite accumulations on the floor of the drift. The term "matte" refers to a named body of standing water in a vertical shaft close to the mine entrance. Error bars were calculated from six to eight repetitions per sample (*23*) and ranged from ±2 to 15%, but were most commonly ±5 to 7%. Sediment numbers refer to cells attached to pyrite surfaces and in associated pore fluids. All Eukarya in these samples were in the solution fraction.

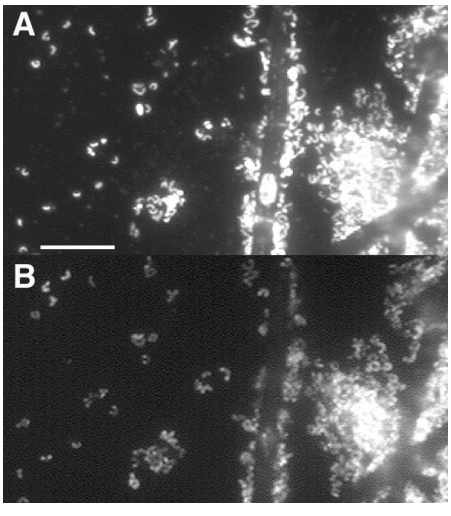

Fig. 2. Probe results for slime from the A drift. (**A**) Slime stained with DAPI. (**B**) Slime stained with LC206 (probe for *L. ferrooxidans*). The filaments on the right-hand side are Eukarya. Scale bar, 5 μm.

pH 0.7 and temperature 42°C) (*11*).

Bacteria were also the predominant form of microbial life (≪5% Archaea or Eukarya) in less extreme environments along the horizontal tunnel into the mine (~20°C, pH 1.3 to 2.4; Fig. 1). However, in contrast to the situation in the pH < 1.0 environments, *T. ferrooxidans* was an important constituent and accounted for about one-third of the total population of pH > 1.0 slime communities. In addition, we successfully cultured *T. ferrooxidans* from these sites with the same standard culture medium used to test for this species in the A drift.

Because *T. ferrooxidans* is (i) not directly associated with the main ore body where primary oxidative dissolution is taking place and (ii) is a common inhabitant only of the more accessible, cooler, higher pH regions, we infer that the impact of this species on pyrite oxidation reactions in the mine is restricted. *Thiobacillus ferrooxidans* may be essentially an opportunist, deriving metabolic energy from dissolved Fe^{2+} but contributing little to acid generation at this site. This conclusion is consistent with the observation that conditions associated with the ore body are below the normal pH and above the normal temperature range for *T. ferrooxidans* (*12*). *Thiobacillus ferrooxidans* still has an important geochemical impact at this site because the oxidation of Fe^{2+} leads to precipitation of ferric iron solids, reducing the metal load in solutions. This potentially beneficial role differs considerably from the negative role often assigned to this species.

Leptospirillum ferrooxidans is extant over most of the range of conditions sampled. Although its distribution suggests that it plays an important ecological role in the microbial community by catalyzing sulfide mineral dissolution, its relative importance in the generation of AMD is not yet known. Our evidence suggests that this species is a dominant planktonic microorganism associated with the ore body, where conditions are generally >40°C and pH is 0.7 to 1.0. *Leptospirillum ferrooxidans* may be the species primarily responsible for catalysis of sulfide oxidation by aqueous ferric iron.

We have sampled the Iron Mountain site throughout the year. Our results show that substantial fluctuations in geochemical conditions are accompanied by variability in microbial population statistics. However, the key conclusions relating to the distribution of *T. ferrooxidans* and *L. ferrooxidans* are valid (*13*).

Although solutions draining most AMD sites have pHs of 2 to 4 (*2*), conditions may typically be more extreme close to reaction sites, as we have observed at Iron Mountain. Sulfuric acid–forming reactions are quite exothermic (*14*), and pHs in proximity to pyrite surfaces are likely much lower than those measured in bulk solution (*2*). Consequently, the organisms that are most important to sulfide dissolution may frequently encounter conditions similar to those found in the tunnels associated with the Iron Mountain ore body. Current models based on *T. ferrooxidans* should be reevaluated to reflect the involvement of different species promoting sulfide weathering by different mechanisms and at different rates.

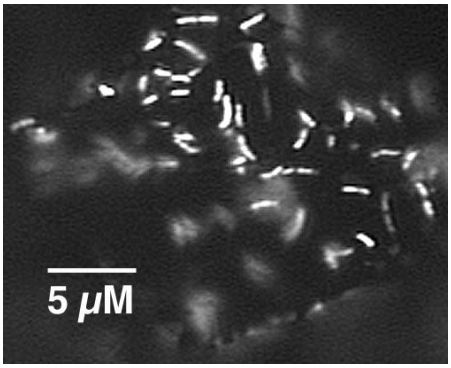

Fig. 3. Bac338 (bacterial probe) to pyrite sediment. The image shows the colonized surface of a pyrite grain from sediment.

REFERENCES AND NOTES

1. C. O. Moses, D. K. Nordstrom, J. S. Herman, A. L. Mills, *Geochim. Cosmochim. Acta* **51**, 1561 (1987); G. W. Luther III, *Aquatic Chemical Kinetics*, W. Stumm, Ed. (Wiley, New York, 1990), p. 173.
2. D. K. Nordstrom and G. Southam, in *Reviews in Mineralogy*, T. R. Banfield and K. H. Nealson, Eds. (Mineralogical Society of America, Washington, DC, 1997), pp. 361–390.
3. P. C. Singer and W. Stumm, *Science* **167**, 1121 (1970).
4. A. R. Colmer and M. E. Hinkle, *ibid.* **106**, 253 (1947); M. P. Silverman and H. K. Ehrlich, *Adv. Appl. Microbiol.* **6**, 153 (1964).
5. H. L. Ehrlich, *Geomicrobiology* (Dekker, New York, ed. 3, 1996), pp. 330–332.
6. U. Helle and U. Onken, *Appl. Microb. Biotechnol.* **28**, 553 (1988); W. Sand, K. Rohde, B. Sobothke, C. Zenneck, *Appl. Environ. Microbiol.* **58**, 85 (1992).
7. M. Vasquez and R. T. Espejo, *Appl. Environ. Microbiol.* **63**, 332 (1997).
8. The *L. ferrooxidans* probes used in this study were based on SSU rRNA gene sequences for 12 *L. ferrooxidans* clones from Iron Mountain (*15*) (LC206: 5′-GGCCATGGGCTCATCTTAAG-3′, *Escherichia coli* positions 206 to 225) and sequences for *L. ferrooxidans* (LF581: 5′-CGGCCTTTCACCAAAGAC-3′, *E. coli* positions 581 to 598) from the Ribosomal Database Project [RDP (*16*)] GenBank (*17*). The probe for *T. ferrooxidans* was based on RDP (*16*) and GenBank (*17*) sequences (TF539: 5′-CAGACCTAACGTACCGCC-3′, *E. coli* positions 539 to 556). Domain-level probes were Bac 338 (5′-GCTGCCTCCCGTAGGAGT-3′, *E. coli* positions 338 to 355), Arch 915 (5′-GTGCTCCCCCGCCAATTCCT-3′, *E. coli* positions 915 to 934), and Euk 502 (5′-ACCAGACTTGCCCTCC-3′, *E. coli* positions 502 to 517) (*18*). Probe sequences were chosen with the oligonucleotide design program OligoFind (*19*). Probes were fluorescently labeled with CY3 (LC206, BAC338, and ARCH915) or 6-FAM (LF581, TF539, and EUK502). Probe specificity was tested with pure cultures of *Aureobasidum pullulans*, *T. ferrooxidans* (ATCC 19859), *L. ferrooxidans* (ATCC 29047), *E. coli* (strain DH5α), and *Sulfolobus solfataricus* (*20*). These cultures were also used as complementary controls in a separate chamber to each individual hybridization performed during the collection of data for this study. The protocol for hybridization to glass slides was adapted from Li *et al.* (*21*), with the concentration of deionized formamide in the hybridization solution as follows: 20% for Euk502 and Bac338 and 25% for LC206, LF581, TF539, and Arch915. Slides were incubated for 7 to 16 hours at 37°C and washed twice in 0.1× saline sodium citrate (15 mM NaCl plus 1.5 mM sodium citrate; 10 min for each wash) and once in autoclaved distilled water (for 5 s).
9. R. I. Amann, W. Ludwig, K.-H. Schleifer, *Microbiol. Rev.* **59**, 143 (1995); P. Weiss, B. Schwetzer, R. I. Amann, M. Simon, *Appl. Environ. Microbiol.* **62**, 1998 (1996); C. R. Woese, *Microbiol. Rev.* **51**, 221 (1987); N. R. Pace, D. A. Stahl, D. J. Lane, G. J. Olsen, in *Advances in Microbial Ecology*, K. C. Marshall, Ed. (Plenum, New York, 1986), pp. 1–55; D. M. Ward, M. M. Bateson, R. Weller, A. L. Ruff-Roberts, in *Advances in Microbial Ecology*, K. C. Marshall, Ed. (Plenum, New York, 1992), pp. 219–286; S. M. Barns, R. E. Fundyga, M. W. Jeffries, N. R. Pace, *Proc. Natl. Acad. Sci. U.S.A.* **91**, 1609 (1994); N. R. Pace, D. A. Stahl, D. J. Lane, G. J. Olsen, *Microb. Ecol.* **9**, 1 (1986).
10. Samples for microbiological analysis were fixed immediately (sediment samples) with 3% paraformaldehyde in phosphate-buffed saline buffer [137 mM NaCl, 2.7 mM KCl, 4.3 mM Na_2HPO_4, and 1.4 mM KH_2PO_4 (pH 7.4)] or stored on wet ice at 4°C (aqueous samples) until concentration and fixation in the laboratory (24 to 48 hours later). Samples were subsequently stored at –20°C in 70% ethanol. Sediment samples were diluted 1:100 in diethyl pyrocarbonate–treated water before application to 0.25% gelatin-coated glass slides. Protocols generally followed Leitch *et al.* (*22*).
11. K. J. Edwards, M. O. Schrenk, J. F. Banfield, R. M. Goodman, Geological Society of America–Abstracts with Programs, Boulder, CO, 28 to 31 October 1996 (Geological Society of America, Boulder, CO, 1996), vol. 28, p. 35; K. J. Edwards, M. O. Schrenk, R. J. Hamers, J. F. Banfield, unpublished data.
12. P. R. Norris, *Microbial Mineral Recovery*, H. L. Ehrlich and C. L. Brierley, Eds. (McGraw-Hill, Hamburg, Germany, 1990), pp. 3–27.
13. K. J. Edwards, T. M. Gihring, M. O. Schrenk, J. F. Banfield, unpublished data.
14. D. K. Nordstrom and J. K. Munoz, *Am. J. Sci.* **287**, 171 (1987).
15. T. M. Rodgers, S. Bintrim, J. F. Banfield, R. M. Goodman, unpublished data; T. M. Rodgers, J. F. Banfield, C. N. Alpers, R. M. Goodman, Seventh Annual V. M. Goldschmidt Conference, Tucson, AZ, 2 to 6 June 1997 (Lunar and Planetory Institute, Houston, TX, 1997), LPI Contribution No. 921, p. 234.
16. B. L. Maidak *et al.*, *Nuceic Acids Res.* **25**, 109 (1997).
17. D. A. Benson , M. Boguski, D. J. Lipman, J. Ostell, *ibid.* **24**, 1 (1996).
18. E. W. Alm, D. B. Oerther, N. Larsen, D. A. Stahl, L. Raski, *Appl. Environ. Microbiol.* **62**, 3557 (1996).
19. J. Ireland, thesis, University of Wisconsin–Madison (1997).
20. The *A. pullulans* culture was supplied by R. Spear, Department of Plant Pathology, University of Wisconsin–Madison; the *T. ferrooxidans* (ATCC 19859, Rockville, MD), *L. ferrooxidans* (ATCC 29047), and *Escherichia coli* (strain DH5α) cultures were supplied by S. Bintrim, Department of Plant Pathology, University of Wisconsin–Madison; and the *S. solfataricus* culture was supplied by A. Tsang, Department of Bacteriology, University of Wisconsin–Madison.
21. S. Li, R. N. Spear, J. H. Andrews, *Appl. Environ. Microbiol.* **63**, 3261 (1997).
22. A. R. Leitch, T. Schwarzacher, D. Jackson, I. J. Leitch, *In-Situ Hybridization; Royal Microscopy So-*

ciety Handbooks (Bios Scientific, Oxford, 1994), vol. 27.
23. Total cell numbers (cells per milliliter) and standard errors (in percent) for Fig. 1. Standard errors are only listed for organisms detected. **A drift: Flow:** 1.8 × 10^6 cells, *L. ferrooxidans* (*Lf*) ±15%, Bacteria (Bac.) ±9%, Eukarya (Euk.) ±2%, Archaea (Arch.) ±2%; **Pool:** 6.3 × 10^4 cells, Bac. ±11%, Euk. ±3%; **Spill.:** 1.4 × 10^6 cells, *Lf* ±12%, Arch. ±2%, Euk. ±5%, Bac. ±8%; **Slime1:** 2.4 × 10^9 cells, *Lf* ±8%, Bac. ±12%, Euk. ±7%; **Slime2**: 1.3 × 10^9 cells, *Lf* ±6%, Bac. ±9%, Euk. ±7%; **Sed.:** 2.2 × 10^7 cells, *Lf* ±4%, Bac. ±6%, Euk. ±2%. **C drift: Flow:** 4.8 × 10^6 cells, *Lf* ±3%, Bac. ±7%; **Spill.:** 5.2 × 10^3 cells, *Lf* ±4%, Bac. ±8%, Arch. ±2%; **Slime:** 4.3 × 10^8 cells, *Lf* ±12%, Bac. ±14%, Euk. ±6%; **Sed.:** 7.3 × 10^5 cells, Bac. ±11%, *Lf* ±2%. **Tunnel: Matte:** 2.4 × 10^5 cells, Bac. ±9%; **Slime1:** 5.7 × 10^9 cells, *Lf* ±5%, *T. ferrooxidans* (*Tf*) ±9%, Bac ±4%; **Slime2**: 3.8 × 10^9 cells, *Lf* ±3%, *Tf* ±8%, Bac. ±6%; **Slime3:** 1.1 × 10^9 cells, *Lf* ±3%, *Tf* ±9%, Bac. ±8%; **Slime4:** 9.1 × 10^9 cells, *Lf* ±6%, *Tf* ±4%, Bac. ±6%; **Slime5:** 4.7 × 10^9 cells, *Lf* ±5%, *Tf* ±9%, Bac. ±5%.
24. We thank T. Rodgers, J. Ireland, C. Alpers, S. Bintrim, and D. K. Nordstrom for their input to this study; S. Bintrim, R. Spear, and A. Tsang for providing cultures; and Iron Mountain Mine Inc. and Stauffer Management Co. for making this work possible. Funding was provided by NSF grant CHE-9521731, EPA grant CR822902–01–0, and a grant from the McKnight Foundation.

13 November 1997; accepted 26 January 1998

Materials with Negative Compressibilities in One or More Dimensions

Ray H. Baughman,* Sven Stafström, Changxing Cui, Socrates O. Dantas

Rare crystal phases that expand in one or more dimensions when hydrostatically compressed are identified and shown to have negative Poisson's ratios. Some of these crystals (i) decrease volume and expand in two dimensions when stretched in a particular direction and (ii) increase surface area when hydrostatically compressed. Possible mechanisms for achieving such negative linear and area compressibilities are described for single crystals and composites, and sensor applications are proposed. Materials with these properties may be used to fabricate porous solids that either expand in all directions when hydrostatically compressed with a penetrating fluid or behave as if they are incompressible.

Most materials contract in all directions when hydrostatic pressure (P) is applied—that is, the volume compressibility ($-dV/VdP$), area compressibilities ($-dA/AdP$), and linear compressibilities ($-dL/LdP$) are all positive. Materials are thermodynamically forbidden to have negative volume compressibilities. A negative area compressibility was initially reported for a trigonal phase of arsenic (*1*), but this result disagrees with later measurements (*2*). However, there are rare reports of crystals having negative linear compressibilities: lanthanum niobate (*3*), cesium dihydrogen phosphate (*4*), an orthorhombic high-pressure paratellurite (TeO_2) phase (*5*), and the isomorphous trigonal Se and Te phases (*6, 7*).

A solid increases density when stretched along an axis of negative linear compressibility, so it is equivalent either to say that a solid has the property of being stretch densified or that it has a negative linear compressibility. If we denote the elastic compliance coefficients for arbitrary orthogonal axes as S_{ij}', then $S_{11}' + S_{12}' + S_{13}'$ is the linear compressibility in the x'-axis direction and $S_{11}' + S_{21}' + S_{31}'$ is the corresponding coefficient for the fractional volume change produced by a uniaxial stress in the x'-axis direction. The elastic constant matrix is symmetric (*8*), so that $S_{ij}' = S_{ji}'$, and therefore these coefficients for pressure-induced linear dimension change and stretch-induced volume change are equal.

By using well-known equations (*8*) for linear compressibility as a function of elastic compliances (S_{ij}), it is easily seen that both the minimum and maximum of linear compressibility occur in crystal-axis directions for orthorhombic or higher symmetry phases. Whereas the existence of only positive linear compressibilities constrains the magnitude of any individual linear compressibility to be less than the bulk compressibility, this constraint disappears if any linear compressibility is negative. We will use experimental data to identify phases where a positive linear compressibility exceeds the bulk compressibility, so the area compressibility (which is the difference between the bulk and the linear compressibility) is negative for a plane perpendicular to the direction of this positive compressibility. This implies that there are negative linear compressibilities for two perpendicular directions within this plane. By choosing a plane with a negative area compressibility as the predominant crystal face, a crystal can be obtained whose total surface area increases with increasing hydrostatic pressure.

We searched for evidence of stretch-densified phases, using the elastic constant tensors that have been experimentally determined for about 500 noncubic crystal phases (*7*). Only about 13 of the 500 investigated compositions are stretch densified (Table 1). Other than the tetragonal mercurous halide phases and the trigonal chalcogen phases, there are no convincing examples of stretch densification in the elastic-constant tabulations for about 270 different hexagonal, tetragonal, and trigonal phases (*7*). Out of 145 tabulated orthorhombic phases (*7*), only cadmium formate, calcium formate, cesium biphthalate, *m*-dihydroxybenzene, 3-methyl 4-nitropyridine 1-oxide, and tris-sarcosine calcium chloride provide data that are clearly consistent with stretch densification. No stretch-densified triclinic phases were identified, and 70 investigated monoclinic phases provide three likely examples of stretch-densified phases: ethylene diamine tartrate, cesium dihydrogen phosphate, and lanthanum niobate.

Each of the stretch-densified crystal phases in Table 1 provides both positive and negative values for the Poisson's ratio, which is the ratio of a lateral contraction to a longitudinal elongation produced by a tensile stress. In fact, Se, the two tetragonal phases, and all three monoclinic phases both increase density and expand in one lateral direction when stretched along a particular direction. However, few crystals with a negative Poisson's ratio have a negative linear compressibility. Equally interesting, a negative area compressibility results for the reported elastic constant tensor (*3, 7*) for monoclinic cesium dihydrogen phosphate and lanthanum niobate, and possibly for orthorhombic cadmium formate.

To enable the design of materials with negative linear compressibilites, we identified several basic structural types that lead to this property. Mechanical and molecular models for hinged structures can be constructed (Fig. 1) in which stretch densification results from a wine-rack–like deformation mode, like those for proposed polydiacetylene carbon phases (*9*). Molecular mechanics calculations suggest (Fig. 1C) (*10*) that ferroelasticity (and associated shape memory behavior) should occur in combination with negative linear compressibilities for particular hinged structures. Both properties are observed for Hg_2Br_2, Hg_2I_2, lanthanum niobate, and tris-sarcosine calcium chloride (*7*). Munn has shown that a negative linear compressibility, combined with a

R. H. Baughman and C. Cui, Allied Signal, Research and Technology, Morristown, NJ 07962–1021, USA.
S. Stafström, Department of Physics and Measurement Technology, Linköping University, S-581 83, Linköping, Sweden.
S. O. Dantas, Departamento de Fisica, UFJF, CEP 36036-330, Juiz de Fora, Minas Gerais, Brazil.

*To whom correspondence should be addressed. E-mail: ray.baughman@alliedsignal.com